RESEARCH ARTICLE

An enhanced version of a bone remodelling model based on the continuum damage mechanics theory.

M. Mengoni[a*] and J.P. Ponthot[a]

[a]*University of Liege (ULg), Department of Aerospace and Mechanical Engineering, MN2L*
(*Received 00 Month 200x; final version received 00 Month 200x*)

The purpose of this work is to propose an enhancement of Doblaré and García's internal bone remodelling model based on the continuum damage mechanics theory. In their paper, they stated that the evolution of the internal variables of the bone microstructure, and its incidence on the modification of the elastic constitutive parameters, may be formulated following the principles of Continuum Damage Mechanics, although no actual damage was considered. The resorption and apposition criteria (similar to the damage criterion) were expressed in terms of a mechanical stimulus. However, the resorption criterion is lacking a dimensional consistency with the remodelling rate. We here propose an enhancement to this resorption criterion, insuring the dimensional consistency while retaining the physical properties of the original remodelling model. We then analyse the change in the resorption criterion hypersurface in the stress space for a 2D analysis. We finally apply the new formulation to analyse the structural evolution of a 2D femur. This analysis gives results consistent with the original model but with a faster and more stable convergence rate.

Keywords: anisotropic bone remodelling; computational biomechanics; model dimensions

1.   Introduction

Bone tissue is an adaptable living structure. It adapts its density and orientation in such a way that its structure is optimized in some sense. It aims at preserving the mechanical properties of the bone and adapting its structure in response to the mechanical demands it experiences. This adaptation process is called bone remodelling. Bone remodelling is usually modelled *in-silico* either following a phenomenological approach, whose goal is to predict the global mechanical behaviour (Jacobs 1994; Doblaré and García 2002; Chen et al. 2007; Schulte et al. 2011), or a mechanobiological approach, whose goal is to predict the evolution of the structure and biological constitution (McNamara and Prendergast 2007; Geris et al. 2010). A bone remodeling algorithm is needed for instance in applications dealing with bone adaptivity such as implants and scaffold design (Terrier et al. 2013; Fernandes et al. 2002; Yeoman et al. 2012; Scannell and Prendergast 2009; Sanz-Herrera et al. 2009; Olivares and Lacroix 2013), prediction the outcome of dentistry or orthodontic treatment (Wang et al. 2012; Field et al. 2012; Mengoni and Ponthot 2010).

García et al. (2001); Doblaré and García (2002) proposed a phenomenological bone remodelling model which, after identifying the internal variables associated to the bone microstructure, follows the anisotropic Continuum Damage Mechanics (CDM) principles (Lemaitre et al. 2000). In the case of bone remodelling, "damage"

---

*Corresponding author. Email: mmengoni@ulg.ac.be Currently at Institute of Medical and Biological Engineering, University of Leeds, UK

has to be understood as a measure of the void volume fraction inside the bone tissue. Contrarily to classical mechanical problems, where damage can only grow, here, thanks to biological processes, the void volume fraction, hence damage, can either grow or decrease (damage repair). The bone tissue at the continuum level is considered as an anisotropic "organization" of elastic trabeculae. The CDM framework is used here not to capture actual damage at the local level, i.e. micro-cracks of the trabeculae, but to represent the bone macroscopic porosity. In terms of morphological data provided by computed tomography, damage is here to be understood as a measure of the bone volume fraction, BV/TV. Its anisotropy is quantified by the fabric second order tensor ($\hat{\mathbf{H}}$) as introduced in the work of Cowin et al. (1985). The damage measure used is therefore virtual and actually reflects the bone density and orientation that can evolve in remodelling situations. The undamaged material is the virtual situation of bone with zero porosity and perfect isotropy. It is the material considered at the trabecular tissue level, assumed to behave in an isotropic linear elastic way. The process of bone resorption corresponds to the classical damage evolution concept, since it increases the void volume fraction and therefore damage (decrease of the density). However, bone apposition can reduce damage and lead to bone repair, which is adequately considered in this extended damage theory.

The aim of this study was to propose enhancements of Doblaré and García's remodelling model in such a way that its dimensional analysis became consistent. The impact of those modifications were then analysed in terms of remodelling surfaces. Finally a 2D remodelling case of a proximal femur was analysed and compared with the original version of the remodelling algorithm.

2.   Remodelling model

2.1   Description of Doblaré and García remodelling's model

García et al. (2001); Doblaré and García (2002) defined a damage tensor, $\mathbf{d}$, used in a strain energy equivalence approach of CDM, by the expression

$$\mathbf{d} = \mathbf{I} - \left(\frac{\rho}{\hat{\rho}}\right)^{\beta/2} \sqrt{A}\hat{\mathbf{H}} = \mathbf{I} - \mathbf{H}^2 \tag{1}$$

where ρ is the apparent density, $\hat{\rho}$ is the density of the ideal bone tissue with null porosity (i.e. 2.1gr/cc), β is the exponent of the power law relating ρ to Young's modulus (β can be function of ρ), and A is a scalar obtained by particularizing the general anisotropic model to the isotropic case (Doblaré and García 2002) for which $d = 1 - \sqrt{E/E_0}$ with E the apparent Young's modulus and E_0 the fully mineralized bone Young's modulus. The damage values increase with a decreasing density. The remodelling tensor $\mathbf{H}$ includes not only the directionality of the bone microstructure through the fabric tensor (it is collinear with $\hat{\mathbf{H}}$), but also the porosity by means of BV/TV. García et al. (2001); Doblaré and García (2002) chose a remodelling stimulus, $\mathbf{Y}$, as the variable thermodynamically conjugated to $\mathbf{H}$:

$$\mathbf{Y} = \left.\frac{\partial \Psi(\boldsymbol{\varepsilon}, \mathbf{H})}{\partial \mathbf{H}}\right|_{\boldsymbol{\varepsilon}=cst} \tag{2}$$

with Ψ being the free energy: $\Psi = \frac{1}{2}\boldsymbol{\sigma} : \boldsymbol{\varepsilon}$, where $\boldsymbol{\sigma}$, and $\boldsymbol{\varepsilon}$ are respectively the Cauchy stress and Cauchy strain tensors.

The damage function is the domain of the stimulus, $\mathbf{Y}$, for which damage is not modified (the lazy zone as used in the literature of bone remodelling). This function is therefore defined by remodelling criteria. García et al. (2001); Doblaré and García (2002), proposed two criteria, one for resorption and one for formation:

$$\text{Resorption: } g_r = \frac{\sqrt{2(1-\mathsf{w})}}{C\hat{\rho}^{-\beta/8}A^{1/8}27^{1/4}}(\mathbf{J}^{-1}:\mathbf{J}^{-1})^{1/4} - \frac{1}{(\psi_\mathsf{t}^\star - \omega)\rho^{(16-5\beta)/8}} \geq 0 \quad (3)$$

$$\text{Formation: } g_f = C\hat{\rho}^{-\beta/8}A^{1/8}\frac{3^{1/4}}{\sqrt{2(1-\mathsf{w})}}(\mathbf{J}:\mathbf{J})^{1/4} - (\psi_\mathsf{t}^\star + \omega)\rho^{(16-5\beta)/8} \geq 0 \quad (4)$$

where $C = n^{1/m}\hat{\rho}^2\sqrt{B}$ (m defines the weighing between the importance of the load intensity and the number of load cycles n such as described in the Stanford remodelling model (Beaupré et al. 1990), B is the proportionality coefficient in the Young's modulus/density relation: $E = B\rho^\beta$), $\psi_\mathsf{t}^\star$ is the reference value of the tissue stress level, 2ω is the width of the so-called lazy-zone of remodelling, and the second order tensor $\mathbf{J}$ is a function of the stimulus $\mathbf{Y}$, that quantifies, through the value of w (w $\in [0,1[$), the relative influence of the hydrostatic (w $= 0$) and deviatoric (w $= 1$) parts of the stimulus in the damage criterion:

$$\boldsymbol{J} = \frac{1}{3}(1-2\mathsf{w})\text{tr}\,(\mathbf{Y})\,\mathbf{I} + \mathsf{w}\mathbf{Y} \quad (5)$$

The damage flow rule is written, according to the thermodynamical approach of damage, as:

$$\dot{\mathbf{H}} = \mu^r\frac{\partial g_r}{\partial \mathbf{Y}} + \mu^f\frac{\partial g_f}{\partial \mathbf{Y}} \quad (6)$$

fulfilling the consistency conditions:

$$\mu^r, \mu^f \geq 0;\ g_r, g_f \leq 0 \text{ and } \mu^r g_r = \mu^f g_f = 0 \quad (7)$$

As (3) and (4) could lead to both the formation and resorption criteria being positive at the same time (unusual case but possible), an arbitrary decision has to be made in that case. García et al. (2001); Doblaré and García (2002) consider that only formation occurs in such a case.

The remodelling rate $\dot{r}$ is obtained from the remodelling criterion that is currently active, i.e.:

$$\dot{r} = \begin{cases} -c_r\dfrac{g_r}{\rho^{2-\beta/2}} & \text{for } g_r \geq 0 \\ 0 & \text{for } g_r < 0 \text{ and } g_f < 0 \\ c_f\dfrac{g_f}{\rho^{2-\beta/2}} & \text{for } g_f \geq 0 \end{cases} \quad (8)$$

Deriving the damage criteria with respect to $\mathbf{Y}$ and using the density evolution defined in the Stanford model (so that the consistency parameters μ^r and μ^f would

4

be function of the apparent density ρ), one finally gets an evolution law for $\mathbf{H}$:

$$\text{Resorption: } \dot{\mathbf{H}}^r = \frac{3\beta k S_v \dot{r}}{4\text{tr}\left(\mathbf{H}^{-2}(\mathbf{W}:\mathbf{J}^{-3})\mathbf{H}\right)}\frac{\hat{\rho}}{\rho}\mathbf{W}:\mathbf{J}^{-3} \tag{9}$$

$$\text{Formation: } \dot{\mathbf{H}}^f = \frac{3\beta k S_v \dot{r}}{4\text{tr}\left(\mathbf{H}^{-2}(\mathbf{W}:\mathbf{J})\mathbf{H}\right)}\frac{\hat{\rho}}{\rho}\mathbf{W}:\mathbf{J} \tag{10}$$

where $\mathbf{W}_{ijkl} = \frac{1}{3}(1-2\text{w})\boldsymbol{\delta}_{ij}\boldsymbol{\delta}_{kl} + \frac{1}{2}\text{w}\left(\boldsymbol{\delta}_{ik}\boldsymbol{\delta}_{jl} + \boldsymbol{\delta}_{il}\boldsymbol{\delta}_{jk}\right)$ is a fourth order pseudo-unit tensor: for w = 1, it is a unit deviatoric tensor, and for w = 0, it is a unit hydrostatic tensor.

Finally, the density rate can be computed as in Beaupré et al. (1990) from

$$\dot{\rho} = k S_v \hat{\rho}\,\dot{r} \tag{11}$$

where kSv is the available specific surface (in mm^2/mm^3).

2.2   Discussion on the dimensional analysis

From (11), it is clear that the dimension of the remodelling rate $\dot{r}$ is a velocity. Indeed $\dot{\rho}$ is a time variation of a density, kS_v is a specific surface, and $\hat{\rho}$ is a density. $\dot{r}$ thus needs to be a time variation of length, i.e. a velocity. Assuming c_r and c_f are both expressed as a velocity per unit stress as found in all their papers on the topic (Doblaré and García 2001, 2002; Pérez. et al. 2010; García et al. 2002; Cegoñino et al. 2004, among others), g_r and g_f need to have identical dimensions so that the remodelling rate has to be expressed with the same units in the resorption or formation cases. From (8), the dimensions of the remodelling criteria need to be defined in such a way that $\dfrac{g_r \text{ or } g_f}{\rho^{2-\beta/2}}$ has the dimensions of a stress, i.e. MPa. However, it is clear from (3) and (4) that it is not the case. Indeed, the dimension of g_f in (4) is a stress$\times\rho^{(16-5\beta)/8}$ (B, $\mathbf{Y}$, $\mathbf{J}$ and $\psi_t^\star$ have the dimensions of a stress; A, n, m have no dimension). The dimension of g_r in (3) is the inverse of the dimension of g_f, i.e. stress$^{-1} \times \rho^{-(16-5\beta)/8}$. These dimensions lead to a remodelling rate whose dimension in formation is a velocity$\times\rho^{-\beta/8}$ and in resorption is a velocity $\times$ stress$^{-2} \times \rho^{-(32-9\beta)/8}$. We propose in this work two modifications that enhance the model so that its dimensions become consistent.

3.   Methods

3.1   Model enhancements

The most straightforward way to address the dimensional issue is to change the dimensions of the remodelling constants c_r and c_f. These two constants would thus be defined with new different dimensions, not as a as a velocity per unit stress any more. Hence the remodelling constants would loose their direct physical meaning, which is an asset of the model proposed in García et al. (2001); Doblaré and García (2002). We thus proposed enhancements to the original model so that the physical meaning of its parameters (c_r and c_f but also A which is defined in such a way that the anisotropic model can be particularized to an isotropic version) were kept.

The first enhancement that can be proposed concerned the resorption criterion. In García et al. (2001); Doblaré and García (2002), it was defined so that the

evolution of the remodelling tensor $\mathbf{H}$ is inversely related to the strain energy density. Choosing however an evolution of the remodelling tensor in the resorption case which is proportional to the strain energy density led to a resorption criterion written as:

$$g_r^{\text{enh.}} = -C\frac{3^{1/4}}{\sqrt{2(1-\mathsf{w})}}\hat{\rho}^{-\beta/8}A^{1/8}(\mathbf{J}:\mathbf{J})^{1/4} + (\psi_{\mathsf{t}}^{\star} - \omega)\rho^{(16-5\beta)/8} \qquad (12)$$

This enhanced resorption criterion has a dimension which is indeed the same as the one of the formation criterion. This alternative definition also prevented the resorption and formation criteria to be simultaneously positive. An arbitrary decision about which criterion should be considered as active in such situation is thus not required any longer. This enhancement of the resorption criterion also involved a change of the remodelling tensor evolution in the resorption case. Following the approach of Doblaré and García (2002) to compute $\dot{\mathbf{H}}^r$ from $g_r^{\text{enh.}}$ actually gives in the present case (Mengoni 2012):

$$\dot{\mathbf{H}}^r = \frac{3\beta k S_v \dot{r}}{4\text{tr}\left(\mathbf{H}^{-2}(\mathbf{W}:\mathbf{J})\mathbf{H}\right)}\frac{\hat{\rho}}{\rho}\mathbf{W}:\mathbf{J} \equiv \dot{\mathbf{H}}^f \qquad (13)$$

Therefore, the same evolution law for the remodelling tensor can be used in both the resorption and formation cases. Only the remodelling rate was modified according to the active remodelling criterion.

The second enhancement that can be applied dealt with the remodelling rate. Keeping the definition of the formation criterion as it is, we modified the remodelling rate in such a way that it was dimensionally consistent with respect to (11):

$$\dot{r}^{\text{enh.}} = \begin{cases} -c_r\dfrac{g_r^{\text{enh.}}}{\rho^{(16-5\beta)/8}} & \text{for } g_r^{\text{enh.}} \geq 0 \\[2mm] 0 & \text{for } g_r^{\text{enh.}} < 0 \text{ and } g_f < 0 \\[2mm] c_f\dfrac{g_f}{\rho^{(16-5\beta)/8}} & \text{for } g_f \geq 0 \end{cases} \qquad (14)$$

This enhanced remodelling rate has the dimension, as expected, of a velocity. Combined with the definition of the enhanced resorption criterion, it retrieved the same remodelling rate for a given stress state as the anisotropic version of the Stanford model presented in Jacobs (1994) from which Doblaré and García's model was derived.

The enhanced resorption criterion hypersurface in the stress plane is analysed and compared to the initial one for a 2D problem in the *Results and Discussion* section.

3.2   *Application to the 2D proximal femur*

The new proposed bone remodelling model was finally applied to analyse the bone structure and density evolution on models of the proximal extremity of a femur submitted to loads representative of a daily normal activity (Beaupré et al. 1990; Jacobs 1994; Doblaré and García 2002; Fernandez et al. 2010, among others). The idea was to assess the capacity of the remodelling algorithm to represent normal density and morphology of the proximal femur submitted to physiological loads, starting from a virtual situation of homogeneous isotropic bone. The two-dimensional model is depicted in Fig. 1 and was used with an in-plane analysis

6

Table 1.   Magnitude and orientation of the applied forces for each load case. Load 1 is a single leg stance, load 2 and 3 represent the extremes of abduction and adduction, respectively. The angle are given with respect to the vertical axis, positive in a clockwise direction (Beaupré et al. 1990).

Load	Cycles per day	Joint reaction (F)		Abductor reaction (R)	
		Magnitude (N)	Orientation (^{o})	Magnitude (N)	Orientation (^{o})
1	6000	2317	24	703	28
2	2000	1158	-15	351	-8
3	2000	1548	56	468	35

Figure 1.   Mesh and boundary conditions used in the 2D model of the proximal femur. On the right is the mesh of the re-enforcing side plate which is superposed to the bone mesh.

(plane strain analysis). This example also served as a verification of the implementation of the model.

The applied loading (Beaupré et al. 1990) represented an approximation of the mean daily loads due to normal gait. The magnitudes, orientations and applied daily cycles of each load are given in Table 1. The load application is done in blocks of 10000 cycles per day, with different frequencies for each case representative of the three different phases of gait. Each load case consisted in a force acting on the femoral head at the articulation (representative of the joint reaction to the leg stance) plus a reaction force induced in the abductor muscle. Each force was distributed on three adjacent mesh nodes as depicted in Fig. 1 in order to decrease load concentration effects. A limitation of this 2D model was pointed out (Jacobs 1994) as the lack of connection between the two cortical layers (lateral and medial parts of the cortex) of the diaphysis, while it appears in reality due to the cylindrical structure of the cortex. Here, we followed the solution used by several authors (Jacobs 1994; Doblaré and García 2002; Fernandez et al. 2010). This consists in including an additional *side plate* (between the four points $ABCD$) of bone tissue, joining both cortical layers. This additional bone tissue is not allowed to remodel. This side plate, when discretized, had its left nodes directly bound to the left nodes of the main model (i.e. the curve AC belongs to both the main model and the side plate) and analogously the right nodes to the right side (i.e. the curve BD belongs to both models), as depicted in Fig. 1. To take into account the fact that the cortical cylinder smoothly merges into the trabecular structure of the metaphysis, the side plate had a varying thickness, from 1mm at the epiphysis to 5mm at the diaphysis, while the main model's thickness is 40mm. This side plate therefore not only connected both cortical layers but also artificially added stiffness to the model. Given that the present work uses a 2D model, the varying thickness is accounted for in a varying stiffness rather than an actual 3D volume.

Finally, a 2mm layer of cartilage was added at the epiphysis and considered as

Table 2.   Remodelling parameters used for the proximal femur adaptation (Doblaré and
García 2002).

Parameter	Value
number of daily load cycles	$n = 10000$
homeostatic value of the stimulus	$\psi^{\star} = 50 \ MPa$
exponent of the stress stimulus	$m = 4$
remodelling velocity for resorption and formation	$c_r = c_f = 0.02 \mu m/(\mathrm{day} MPa)$
half-width of the lazy zone	$\omega = 25\% \psi^{\star}$

a simple elastic material, with a Young's modulus of 5.9GPa and a Poisson's ratio
of 0.47 (Beaupré et al. 1990), see Fig. 1.

The initial situation corresponded to an isotropic homogeneous state with initial
density $\rho = 0.5gr/cc$. The loads were applied for 300 consecutive days. The set
of remodelling parameters presented in Table 2 was used (equivalent to the set
of parameters used in Doblaré and García (2002)). The density over time given
by both versions of the remodelling algorithm were compared in terms of spatial
distribution and local density change. The trabecular bone orientation was assessed
by looking at stiffness ellipses, i.e. at a plane representation of the 3D stiffness
matrix.

Both the original version of the remodelling criteria and the enhanced one have
been implemented into the non-linear implicit finite element code Metafor (devel-
oped at the LTAS/MN2L, University of Liége, Belgium - www.metafor.ltas.ulg.ac.
be) used in this work.

4.   Results and Discussion

4.1   Modifications of the resorption criterion

The resorption criteria are first compared in terms of their graphical representation
in the principal stress space (in all the figures, σ_1, σ_2 are the principal stresses
in MPa). All the presented data assume a remodelling case with the following
parameters: initial density $\rho = 1gr/cc$ and remodelling parameters as in Table 2.

Both versions of the remodelling criterion lead to a remodelling rate in resorption
that increases as the stress decreases. In the isotropic case (w = 0), it can be easily
demonstrated that both versions of the resorption criterion (3 and 12) are set to
zero for the same stress values. Thus in this case, the two formulations have identi-
cal zero-level surfaces, represented by simple ellipses in the stress space (Figure 2).
However, the values taken by the resorption criteria for other given values of the
principal stresses σ_1, σ_2 are completely different. The original resorption criterion
is shaped like a hyperbolic funnel, i.e. a concave 3D surface, with an infinite posi-
tive value at the origin, while the shape of the enhanced version is a wide parabolic
cone, i.e. a convex 3D surface, with a finite positive value at the origin, (Figure 3).
Except in the vicinity of the zero stress state, the enhanced version thus gives higher
values of the criterion than the original one but these values remain limited as the
stresses decrease. In the isotropic case, the remodelling rate in resorption will thus
be activated at the same stress level for both formulations. However, the enhanced
formulation leads to a higher remodelling rate than the original version, except in
the vicinity of a zero stress state where the original formulation leads to a singular-
ity. Even tough from a physiological point of view a zero stress state never arises in
the bone, it does computationally. Indeed, most remodelling algorithms (Fernandes
et al. 1999; Doblaré and García 2002; McNamara and Prendergast 2007; Chen et
al. 2007; Schulte et al. 2011) are used on bones submitted to loading starting from
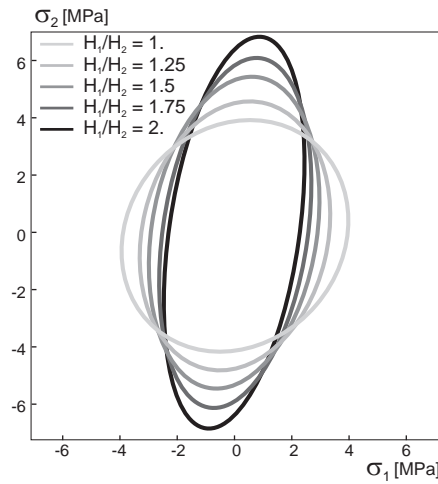a fictitious state of an homogeneous isotropic bone without any initial stresses.

8

Figure 2. Representation of the resorption criteria zero-level curve in the stress space for a 2D problem for different values of the ratio of the fabric tensor eigenvalues H_1/H_2 in the isotropic case: w = 0.
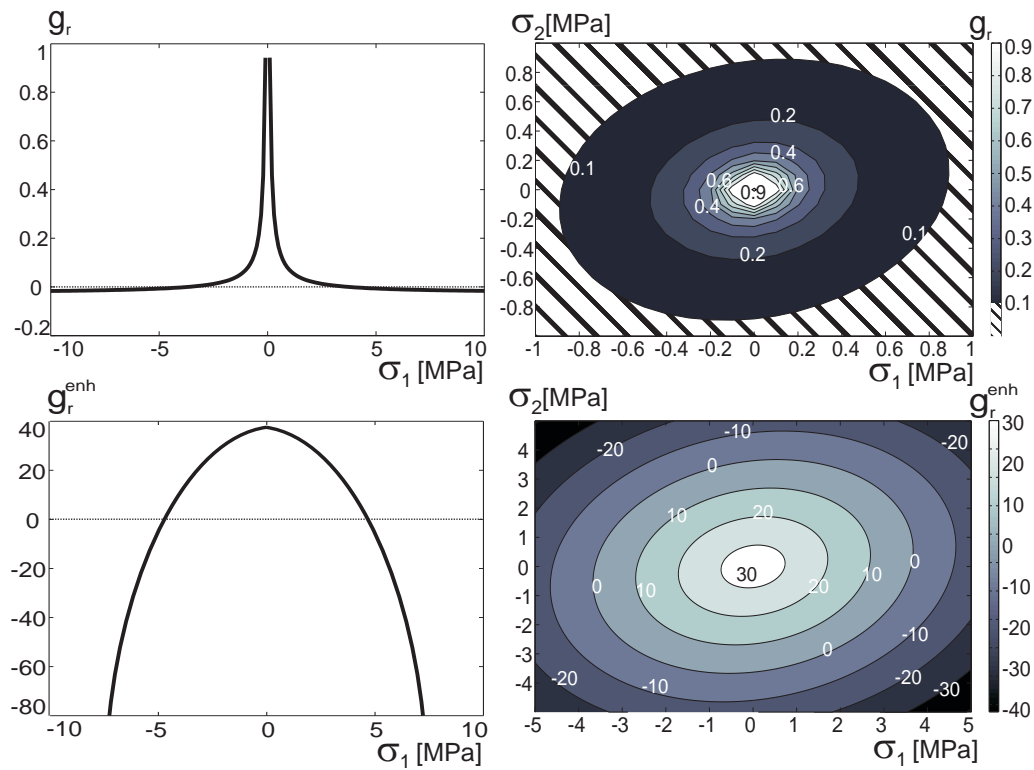

Figure 3. Representation of the resorption criteria in the stress space for a 2D problem in the isotropic case: w = 0. Top panel is the original version of the resorption criterion, bottom panel is the enhanced version. Left: shape of the criteria for $\sigma_2 = 0$; Right: σ_1, σ_2 contours of the criteria (for the original criterion, values below 0.1 are hatched for visibility, the value at $(0,0)$ is infinite). Beware of the scale differences between the figures.

Thus, when the remodelling algorithm is fully embedded in the constitutive law as it is the case here, the stimulus is first evaluated on a zero stress configuration, and would lead to an infinite bone resorption.

In the anisotropic case (w $\in]0, 1[$), the shape of the zero-level of each resorption criterion formulation differs more and more with larger values of w (Figure 4). The area of positive values of the criterion increases with increasing values of w for the original version of the criterion while it decreases for the enhanced version. In par-
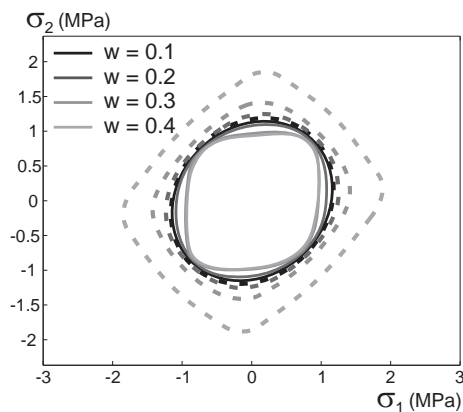
Figure 4. Representation of the resorption criteria zero-level curve in the stress space for a 2D problem in the anisotropic case for different values of w and for a ratio of the fabric tensor eigenvalues $H_1/H_2 = 2$. Plain curves are for the enhanced version of the criterion, dashed curves are for the original one.
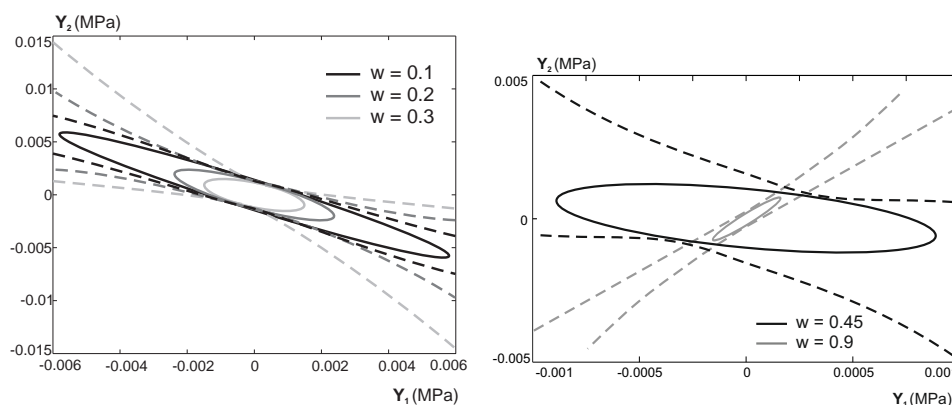

Figure 5. Representation of the resorption criteria zero-level curve in the damage stimulus space (Y_1 and Y_2 are the eigenvalues of the damage stimulus tensor $\mathbf{Y}$) for a 2D problem in the anisotropic case for different values of w. Plain curves are for the enhanced version of the criterion, dashed curves are for the original one. Note the loss of convexity in the original resorption criterion and a change of directionality for values of w>0.5.

ticular, the original resorption criterion loses convexity while the enhanced version preserves the convexity of the resorption criterion (Figure 5 and appendix A) in the damage stimulus space. This loss of convexity is important with respect to the fact that, in Doblaré and García (2002), the authors show that if the formation and resorption criteria remain convex, then a minimum mechanical dissipation principle is fulfilled. Finally, both zero-level representation of the criterion have the same orientation in the stress space with increasing values of the ratio H_1/H_2 (Figure 6).

4.2   Application to the 2D proximal femur

The model performance is first assessed by comparing the bone density after 100 and 300 days of application of the daily loading cycles with results obtained using Doblaré and García (2002) original model. The aim is to show that the models can produce the main morphological features of an actual proximal femur, within the same range of density values. These features are a cortical formation in the medial and lateral part of the diaphysis (thicker at the medial part), a decrease of the density in the intramedullary canal, a region of higher density in the proximal part of the femoral neck, a head bounded by two low density regions as well as a reduced density in the area referred to as Ward's triangle.

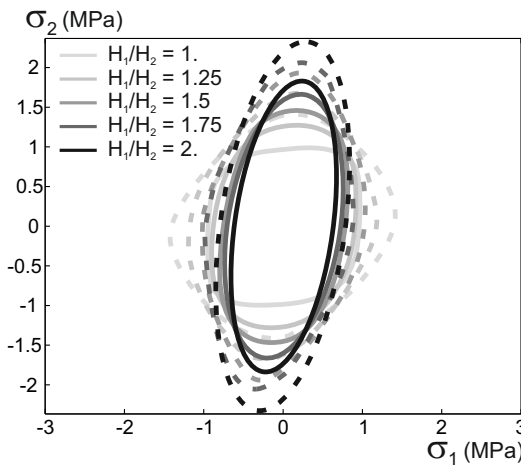Figure 7 shows that the proposed model can reproduce the main features of the

10

Figure 6.   Representation of the resorption criteria zero-level curve in the stress space for a 2D problem for different values of the ratio H_1/H_2 in the anisotropic case: w = 0.3. Plain curves are for the enhanced version of the criterion, dashed curves are for the original one.

proximal femur morphology at least as well as the original model. In particular, Ward's triangle is clearly present, even after a simulation corresponding to only 100 days of remodeling. The other described features are also present after a simulation of 100 days, except for the lateral cortical layer at the diaphysis. The intramedullary canal is well defined, as is the region of higher density at the proximal neck. After a simulation of 300 days, the lateral cortical layer at the diaphysis is also present. The reduction of density goes down to 0.1gr/cc (at the intramedullary canal, the region of Ward's triangle, and the regions of the head). This lower bound is higher than the original one, which goes down to 0.05gr/cc, i.e. the lowest authorized bound. Similarly, the densest areas in the original model reach the maximal authorized density of 2.05gr/cc while the maximal density of the enhanced model is 2.0gr/cc. Figure 8 shows the density variation at five different locations. At the beginning of the simulation, the stress is null everywhere, there is thus formation of bone everywhere. After the application of a few force cycles, resorption in low stress areas is higher for the enhanced model than for the original one for a given state of stress as the original version has a remodeling criterion with lower values than the enhanced version. The formation areas thus bear even more load for the enhanced model and increase the formation rate. Eventually, for most areas, the density tends toward a similar value for both formulations of the resorption criterion. The enhanced model however converges towards that end value faster than the original one.

   The model performance is also assessed by comparing the orientation of the trabecular bone. The bone orientation is assessed by looking at stiffness ellipses. Their orientation reflects the trabecular orientation and their axis lengths the bone density in the two principal directions. Both models show the same orientations over the whole proximal femur (Figure 9). Particularly, the bone tissue is oriented along the diaphysis on its cortical sides, towards the proximal head in the stronger part of the head and is pretty much isotropic in the mediaphysis and the intramedullary canal. As discussed previously, the bone is denser for the original model, it is thus stiffer. As a consequence, the stiffness ellipses, even tough they show similar, but not identical everywhere, orientation, have longer axis lengths for the original model than for the enhanced version.

   Finally, Figure 10 shows the convergence of the models in terms of the total mass variation. The enhanced model converges in a smoother way than the original one which exhibits a higher tendency to oscillate around a null variation for a longer period of time. Those oscillations are not related to the daily alternation of load
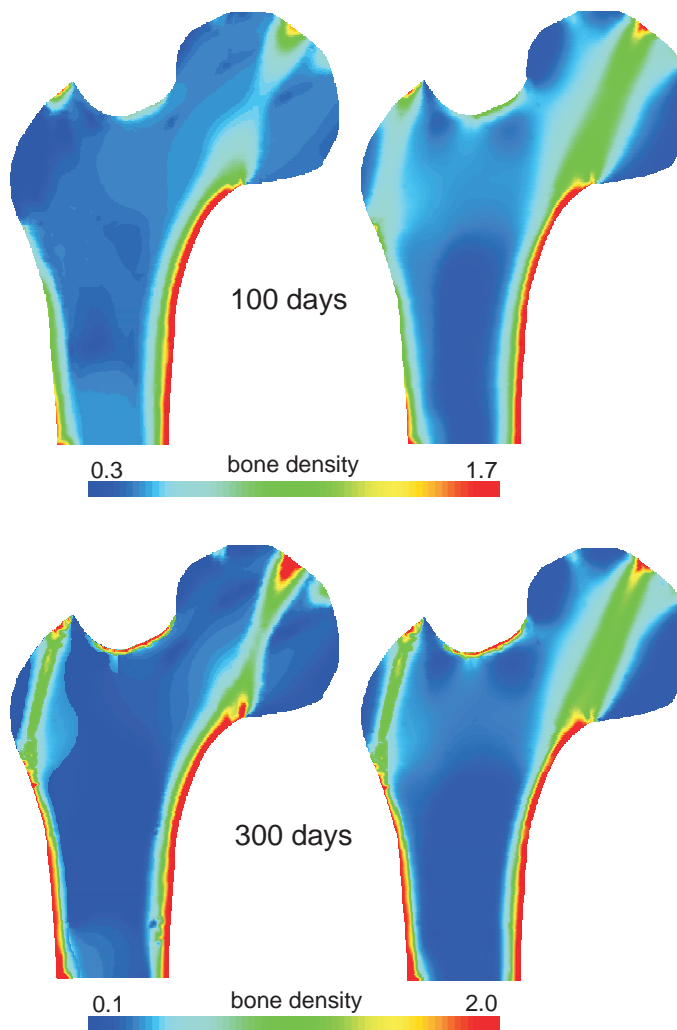
Figure 7.   Bone density maps after 100 (top) and 300 (bottom) days of remodeling simulation. Comparison between original formulation (left) and the enhanced one (right).
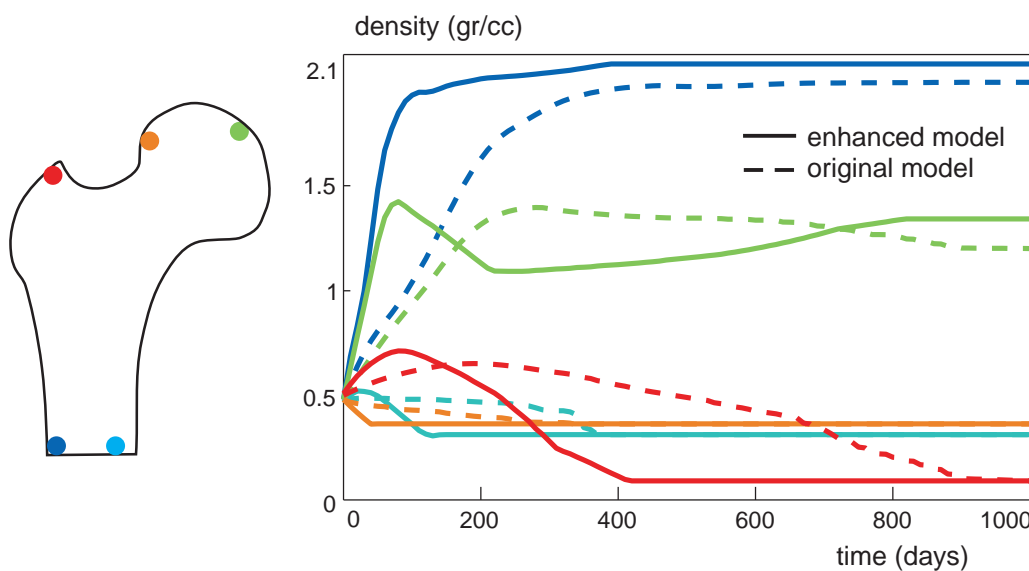

Figure 8.   Bone density vs. time at five different locations during the remodeling simulation. The left schematic shows the color-coded locations plotted on the right.
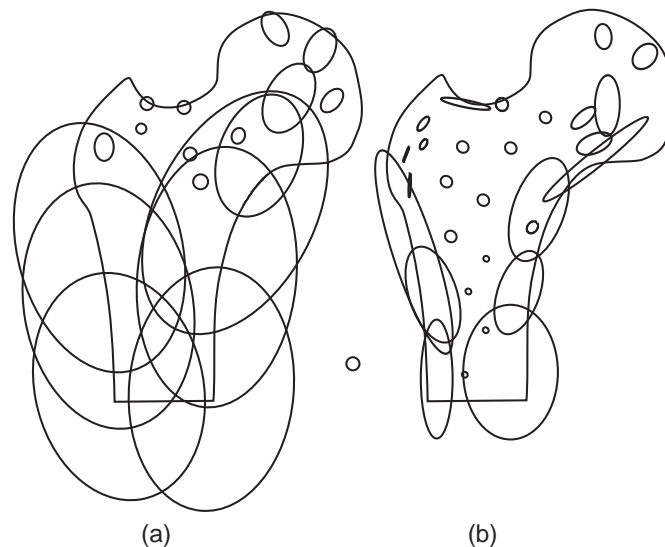
12

Figure 9. Trabecular bone orientation after a simulation of 300 days. The ellipses represent the stiffness value, a 1GPa isotropic stiffness circle indicator is also depicted in the middle of the two figures. (a) results by the original model Doblaré and García (2002), and (b) the enhanced model.
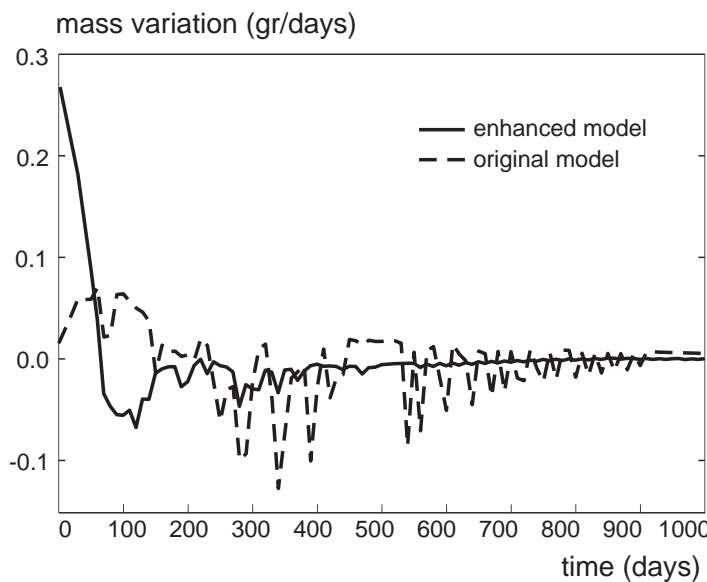

Figure 10. Mass variation of the proximal femur vs. time.

cases (3 load cases a day, for a total of 10000 cycles per day) as they present a period longer than a day. While the enhanced model does not evolve much in terms of mass after 450 days, it takes the original model twice as long to reach a null mass variation.

5.   Conclusion

García et al. (2001); Doblaré and García (2002) proposed a thermodynamically consistent model for bone internal remodelling. They established a model based on the principles of Continuum Damage Mechanics. Their model elegantly proposes a framework to combine the anisotropy of the bone morphology through macroscopic measures such as the fabric tensor and the apparent density while allowing an

adaptation of both these morphological parameters. The model assimilates the bone voids with the microcracks of other material damage models. It changes some of the standard assumptions in the continuum damage theory to adapt it to the special requirements of living adaptive materials, especially the possibility of decreasing the damage level (repair) by providing the required metabolic energy.

However, we showed that the initially proposed model contained inconsistencies in its dimensional analysis. We thus here propose an enhancement of the model, in particular for the resorption criterion. If an isotropic remodelling is considered, no change is observed on the values of the stresses for which the resorption criterion exhibits a zero value. However, the value of the criterion for any other stress intensities is completely different between the original version of the criterion and the enhanced one presented here. For the anisotropic case, while the formation criterion is convex in the remodelling stimulus space, the original resorption criterion is not. Therefore, the minimum mechanical dissipation principle is not fulfilled. The enhanced version of the resorption criterion however ensures the convexity of the criterion in all situations. On a 2D model of the proximal femur submitted to gait cycles, both versions of the model converge towards the same density distribution. The enhanced version reaches this converged state twice as fast as the original one. Moreover, it presents a much less pronounced tendency to exhibit oscillations.

Appendix A. On the convexity of the resorption criteria

A function is convex if it is defined over a convex domain and its Hessian operator, $\mathbf{H}$, is positive definite. Concerning the resorption criteria, the convexity in the convex $\mathbf{Y}$ space is needed, the Hessian operator for each criteria in that space are computed hereafter:

$$\mathbf{H}_{ijkl}^{\texttt{Dob.}} = \frac{\partial^2 g_r^{\texttt{Dob.}}}{\partial Y_{ij} \partial Y_{kl}} \text{ and } \mathbf{H}_{ijkl}^{\texttt{enh.}} = \frac{\partial^2 g_r^{\texttt{enh.}}}{\partial Y_{ij} \partial Y_{kl}}$$

For the initial criterion, the first derivative is written as:

$$\frac{\partial g_r^{\texttt{Dob.}}}{\partial \mathbf{Y}} = -\frac{\alpha}{2} (\mathbf{J}^{-1} : \mathbf{J}^{-1})^{-3/4} \mathbf{W} : \mathbf{J}^{-3}$$

where $\alpha = \dfrac{\sqrt{2(1-\mathrm{w})}}{C \hat{\rho}^{-\beta/8} A^{1/8} 27^{1/4}} > 0$. The Hessian operator is thus

$$\mathbf{H}_{ijkl}^{\texttt{Dob.}} = -\frac{\alpha}{2} (\mathbf{J}^{-1} : \mathbf{J}^{-1})^{-3/4} \left[\frac{3}{2} (\mathbf{J}^{-1} : \mathbf{J}^{-1})^{-1} (\mathbf{W} : \mathbf{J}^{-3})_{ij} (\mathbf{W} : \mathbf{J}^{-3})_{kl} - \mathbf{Z}_{ijkl} \right]$$

where $\mathbf{Z}_{ijkl} = \mathbf{W}_{ijmn} \left(J_{om}^{-1} J_{pn}^{-3} + J_{om}^{-2} J_{pn}^{-2} + J_{om}^{-3} J_{pn}^{-1} \right) \mathbf{W}_{klop}$

For the new proposed criterion, the first derivative is written as:

$$\frac{\partial g_r^{\texttt{enh.}}}{\partial \mathbf{Y}} = -\frac{\gamma}{2} (\mathbf{J} : \mathbf{J})^{-3/4} \mathbf{W} : \mathbf{J}$$

where $\gamma = C \dfrac{3^{1/4}}{\sqrt{2(1-\mathsf{w})}} \hat{\rho}^{-\beta/8} A^{1/8} > 0$. The Hessian operator is thus

$$\mathsf{H}_{ijkl}^{\mathtt{Dob.}} = \frac{\gamma}{2}(\mathbf{J}:\mathbf{J})^{-3/4} \left[\frac{3}{2}(\mathbf{J}:\mathbf{J})^{-1}(\mathbf{W}:\mathbf{J})_{ij}(\mathbf{W}:\mathbf{J})_{kl} - \underbrace{\mathbf{W}_{ijop}\mathbf{W}_{klop}}_{\mathsf{X}_{ijkl}} \right]$$

In the case for which only the hydrostatic part of the stimulus has an influence on the damage variation, $\mathsf{w} = 0$, thus:

$$\mathbf{J} = j\mathbf{I}, \ \mathbf{J}:\mathbf{J} = 3j^2, \ \mathbf{J}^{-1}:\mathbf{J}^{-1} = 3j^{-2}$$

$$\mathbf{W}:\mathbf{J} = j\mathbf{I}, \ \mathbf{W}:\mathbf{J}^{-3} = j^{-3}\mathbf{I}$$

$$\mathsf{X}_{ijkl} = \frac{1}{3}\delta_{ij}\delta_{kl}, \ \mathsf{Z}_{ijkl} = j^{-4}\frac{1}{3}\delta_{ij}\delta_{kl}$$

In that case, it is straightforward to show that:

$$\mathsf{H}_{ijkl}^{\mathtt{Dob.}} = -\underbrace{\frac{1}{6}\frac{\alpha}{2}(3j^{-2})^{-3/4}}_{>0}\delta_{ij}\delta_{kl}$$

which is not definite positive.

And that

$$\mathsf{H}_{ijkl}^{\mathtt{enh.}} = \underbrace{\frac{1}{6}\frac{\gamma}{2}(3j^2)^{-3/4}}_{>0}\delta_{ij}\delta_{kl}$$

which is definite positive.

For this simple hydrostatic case, the original criterion is thus not convex while the enhanced one is.

References

Beaupré GS, Orr TE, Carter DR. 1990. An approach for time-dependent bone modeling and remodeling-theoretical development. Journal of Orthopedic Research 8(5):651–661.

———. 1990. An approach for time-dependent bone modeling and remodeling-application: a preliminary remodeling simulation. Journal of Orthopedic Research 8(5):662–670.

Cegoñino J, García-Aznar JM, Doblaré M, Palanca D, Seral B, Seral F. 2004. A comparative analysis of different treatments for distal femur fractures using the finite element method. Computer Methods in Biomechanics & Biomedical Engineering 7(5):245–256.

Chen G, Pettet G, Pearcy M, McElwain D. 2007. Modelling external bone adaptation using evolutionary structural optimisation. Biomechanics and Modeling in Mechanobiology 6(4):275–285.

Cowin SC, Hart RT, Balser JR, Kohn DH. 1985. Functional adaptation in long bones: establishing in vivo values for surface remodeling rate coefficients. Journal of Biomechanics 18(9):665–684.

Doblaré M, García JM. 2001. Application of an anisotropic bone-remodelling model based on a damage-repair theory to the analysis of the proximal femur before and after total hip replacement. Journal of Biomechanics 34:1157–1170.

———. 2002. Anisotropic bone remodelling model based on a continuum damage-repair theory. Journal of Biomechanics 35(1):1–17.

Fernandes P, Rodrigues H, Jacobs C. 1999. A Model of Bone Adaptation Using a Global Optimisation Criterion Based on the Trajectorial Theory of Wolff. Computer Methods in Biomechanics & Biomedical Engineering 2(2):125–138.

Fernandes P, Folgado J, Jacobs C, Pellegrini V. 2002. A contact model with ingrowth control for bone remodelling around cementless stems. Journal of biomechanics 35(2):167–176.

Fernandez J, García-Aznar J, Martínez R, Viaño J. 2010. Numerical analysis of a strain-adaptive bone remodelling problem. Computer Methods in Applied Mechanics and Engineering 199:1549–1557.

Field C, Li Q, Li W, Thompson M, Swain M. 2012. A comparative mechanical and bone remodelling study of all-ceramic posterior inlay and onlay fixed partial dentures. Journal of dentistry 40(1):48–56.

García JM, Doblaré M, Cegoñino J. 2002. Bone remodelling simulation: a tool for implant design. Computational Materials Science 25(1-2):100–114.

García JM, Martinez MA, Doblaré M. 2001. An Anisotropic Internal-External Bone Adaptation Model Based on a Combination of CAO and Continuum Damage Mechanics Technologies. Computer Methods in Biomechanics & Biomedical Engineering 4:355 – 377.

Geris L, Vander Sloten J, Van Oosterwyck H. 2010. Connecting biology and mechanics in fracture healing: an integrated mathematical modeling framework for the study of nonunions. Biomechanics and Modeling in Mechanobiology 9(6):713–724.

Jacobs CR. 1994. Numerical simulation of bone adaptation to mechanical loading PhD Thesis. Department of Mechanical Engineering - Stanford University.

Lemaitre J, Desmorat R, Sauzay M. 2000. Anisotropic damage law of evolution. European Journal of Mechanics - A/Solids 19(2):187–208.

McNamara LM, Prendergast PJ. 2007. Bone remodelling algorithms incorporating both strain and microdamage stimuli. Journal of biomechanics 40(6):1381–1391.

Mengoni M. 2012. On the development of an integrated bone remodeling law for orthodontic tooth movements models using the Finite Element Method. PhD Thesis. School of Engineering, University of Liège, Belgium. http://orbi.ulg.ac.be/handle/2268/126082.

Mengoni M, Ponthot JP. 2010. Isotropic continuum damage/repair model for alveolar bone remodeling. Journal of computational and applied mathematics 234(7):2036–2045.

Olivares AL, Lacroix D. 2013. Computational Methods in the Modeling of Scaffolds for Tissue Engineering. In: Computational Modeling in Tissue Engineering. Springer. pp. 107–126.

Pérez. MA, Fornells P, Doblaré M, García-Aznar JM. 2010. Comparative analysis of bone remodelling models with respect to computerised tomography-based finite element models of bone. Computer Methods in Biomechanics & Biomedical Engineering 13(1):71–80.

Sanz-Herrera J, García-Aznar J, Doblaré M. 2009. On scaffold designing for bone regeneration: a computational multiscale approach. Acta Biomaterialia 5(1):219–229.

Scannell PT, Prendergast PJ. 2009. Cortical and interfacial bone changes around a non-cemented hip implant: simulations using a combined strain/damage remodelling algorithm. Medical engineering & physics 31(4):477–488.

Schulte FA, Lambers FM, Webster DJ, Kuhn G, Müller R. 2011. In vivo validation of a computational bone adaptation model using open-loop control and time-lapsed micro-computed tomography. Bone 49(6):1166–1172.

Terrier A, Larrea X, Guerdat J, Crevoisier X. 2013. Development and validation of a numerical model for tibial component analysis in total ankle replacement. Computer Methods in Biomechanics and Biomedical Engineering 16(sup1):249–250.

Wang C, Han J, Li Q, Wang L, Fan Y. 2012. Simulation of bone remodelling in orthodontic treatment. Computer Methods in Biomechanics and Biomedical Engineering e-pub ahead of print(0):1–9. PMID: 23148454

Yeoman M, Lowry C, Cizinauskas A, Vincent G, Simpson D, Collins S. 2012. Bone Remodelling Following THR; Shorts Stems Are Less Likely to Lead to Bone Resorption. Journal of Bone & Joint Surgery, British Volume 94(SUPP XL):177–177.